Characterization of Hypervelocity Impact Debris from the DebriSat Tests

Paul M. Adams, Patti M. Sheaffer, Zachary Lingley and Gouri Radhakrishnan
The Aerospace Corporation, 2310 East El Segundo Blvd., El Segundo, CA 90245

ABSTRACT

The DebriSat program consisted of 3 hypervelocity impact tests conducted in 2 Torr of air with 7 km/s, 600 g aluminum projectiles. In the first test, Pre Preshot, the target consisted of multiple layers of fiberglass, stainless steel and Kevlar fabric. No soft catch foam was used. The subsequent two tests, DebrisLV and DebriSat, were designed to simulate hypervelocity impacts with a launch vehicle upper stage and a modern LEO satellite, respectively. The interior of the chamber was lined with soft catch foam to trap break-up fragments. In all three tests, witness plates were placed near the target to sample impact debris and determine its reflectance, composition and spectral properties. Reflectance measurements are important for calculating the size of orbital hypervelocity impact fragments.

The debris from the Pre Preshot test consisted of a two-phase mixture formed from solidified molten silicate and steel droplets. Individual droplets ranged from 100 μm to 10 nm. The reflectance of witness plates dropped from 95% to 20-30% as a result of the debris. Debris collected on witness plates in the DebrisLV and DebriSat tests consisted of μm to nm-sized solidified molten metallic droplets in a matrix of condensed vaporized soft catch. Disordered graphitic carbon was also detected. The reflectance of debris-covered witness plates dropped from 95% to 5%. The dramatic decrease in reflectance for hypervelocity impact debris is attributed to the effect of scattering from μm to nm sized solidified molten metallic droplets and the presence of graphitic carbon, when organics are present. The presence of soft catch in the later tests and the high organic content with graphitic carbon in the debris appear to be responsible for this much lower post-test reflectance. Understanding orbital debris reflectance is critical for estimating size and determining debris detectability.

1. INTRODUCTION

The size of debris tracked by the U. S. Space Surveillance Network is determined by radar cross section (RCS). However, the lower size limits of objects that can be tracked and their size inferred by RCS are on the order of 10 cm for LEO and 1 m in GEO [1]. The primary causes of orbital debris breakups are explosions and impacts. In order to obtain data on the physical properties of impact generated fragments smaller than 10 cm a series of laboratory-based impact experiments were conducted by NASA and the Department of Defense (DoD) in the early 1990s. The Satellite Orbital-Debris Characterization Impact Test 4 (SOCIT-4) [2-5] involved a Navy Transit satellite bus and produced the dataset that was used to develop the current NASA/DoD satellite breakup models [6]. In 2007 China successfully tested an antisatellite weapon on the FY-1C weather satellite and in 2009 there was a collision between the Iridium 33 and Cosmos 2251 satellites. The current NASA breakup model was relatively successful in predicting the impact debris fragments of Cosmos 2251, which was an older satellite. It was significantly less effective in describing the impact fragment distributions of FY-1C and Iridium 33, which are of much more recent construction using materials not used in Transit or Cosmos 2251 [1]. As a result, the DebriSat tests were conducted to better understand the distribution of fragments generated from a hypervelocity impact with a modern satellite constructed from current materials [1].

The DebriSat series of tests (Pre Preshot, DebrisLV, and DebriSat) were a NASA program with support/collaboration from the Air Force Space and Missile Systems Center, University of Florida and the Aerospace Corporation. Tests were conducted in 2014 in nominally 2 Torr of air at the Arnold Engineering Development Complex (AEDC) Range G Two-Stage Light Gas Gun Facility which utilizes a 3 m diameter vacuum chamber [7, 8]. All three tests used a 580 gram, 8.6 cm diameter x 10.3 cm long, hollow aluminum cylinder with a Nylon sleeve as the projectile with a nominal velocity of 6.8 km/sec. [7]. For the DebrisLV and DebriSat tests the chamber was lined with specially redesigned “soft catch” foam panels which were used to trap the impact fragments for size distribution analysis [9].

A combination of radar and optical telescope photometry data has been used to determine the trackable orbital debris population. From extremely short arc optical observations of an object an angular velocity can be obtained. Assuming a circular orbit the range can be calculated, which combined with the apparent brightness and solar phase function the object size can be calculated, if an albedo is assumed [10]. Conversely if the object size can be determined from its RCS the albedo can be calculated. Assumptions about an object's shape and composition can affect RCS estimates and albedo variations within a population can introduce large random errors in albedo calculations. To compensate for these errors a large number of observations are made in order to obtain a statistically significant sampling from which a more accurate estimate of an average albedo can be obtained. A wide range of albedos have been published [10-17] (Table 1) for a variety of orbital debris, some of which are contradictory and counterintuitive. As a result of some of these studies it has been concluded that "more research is required" into determining a global albedo value [10] which ultimately determines the lower size limit of an object that can be determined from its RCS.

There is limited laboratory evidence that impact debris have a thin coating of soot from the breakdown of plastics in circuit boards [11]. While there has been documentation of the size distribution of fragments generated in the SOCIT-4 test there has been little to no description of the appearance of fragments [2-4]. The only mention was that soot consisting of particles < 50 μm was present [3]. Early measurements of the average albedo of satellite debris range from 0.042-0.196 for various fragmentation scenarios with a value of 0.065 for hypervelocity impacts (Table 1) [11]. It has also been suggested that the albedo of orbital debris may be used to determine the method of breakup (explosion vs. impact) [11]. To address these issues we fielded witness plates in all three DebriSat hypervelocity impact tests in order to collect microscopic debris coatings and to determine their physical characteristics (particle size distribution, chemistry and optical properties). This will help us better understand how these coatings form and let us obtain direct albedo measurements from hypervelocity impact debris for comparison with reported global values derived from radar cross section and apparent brightness..

Table 1. Summary of Orbital Debris Albedo Estimates

	Albedo	Object(s)	Cause	Comments
Ref. [11]	0.196 0.103 0.087 0.065 0.042	Ariane 3rd stage Landsat 1 Cosmos 1275 Solwind Landsat 3	Unknown Propellant explosion Unknown Hypervelocity impact Propellant explosion	
Ref. [12]	0.08	Global mean	Global/undetermined	
Ref. [13]	0.01-0.18	13 satellites	Undetermined	IR photometry
Ref. [14]	0.09 (median) 0.24 (median)	7 breakups Spot1/Viking	Mixed Undetermined	
Ref. [16]	0.13	Fragmentation only	Fragmentation only	global
Ref. [17]	0.175 (0.185)	Fragmentation only	Fragmentation only	Global, reprocessed 2007 data
Ref. [10]	0.145/0.209/0.275 0.095/ 0.142	Fragmentation only Non-fragmentation	Fragmentation only Non-fragmentation	Mean / Average/ Bias corrected Mean, Average,

2. LABORATORY EXPERIMENTAL

For the DebrisLV and DebriSat tests approximately twenty four 1 cm diameter aluminum pin-mount scanning electron microscope (SEM) stubs were inserted into the surface of the soft catch prior to the test. Those in the DebriSat tests had a sheet of tantalum on the surface to help distinguish Al from the target/projectile from the SEM stub. The stubs were arranged both up-range and down-range of the targets at four azimuthal locations. Post-test selected stubs were examined in a JEOL 7600F field emission SEM equipped with an Oxford X-Max SDD energy dispersive spectrometer (EDS). Specimens were prepared for transmission electron microscopy (TEM) by wiping the surface of witness plates with ultra-carbon coated lacey-carbon TEM grids. They were examined in a JEOL model 3100 TEM/STEM equipped with an Oxford INCA x-sight EDS. TEM imaging was performed at 300 kV in bright field phase contrast mode. Raman spectroscopy of impact deposits was performed with a Renishaw inVia spectrometer using a 514 nm Ar-ion laser. Fourier transform infrared (FTIR) spectroscopy (2.5-25 μm) was performed with a

Thermo Nicolet model 6700 spectrometer equipped with DTGS and MCT-A detectors. Qualitative biconical and quantitative hemispherical diffuse reflectance measurements were made with a Harrick Scientific Praying Mantis accessory and a Labsphere 3" diameter Au integrating sphere, respectively. Labsphere Infragold was used as the background reference for both reflectance measurements. An Agilent Technologies model 4100 Exoscan portable FTIR was used to obtain *in situ* diffuse reflectance spectra from the surfaces of various materials used to construct DebrisLV and DebriSat prior to, and immediately after the tests [18].

3. PRE PRESHOT TEST

In preparation for the DebriSat hypervelocity impact test a Pre Preshot was conducted to validate the performance of the specially designed aluminum projectile to meet the velocity goal of ~7 km/s and confirm operational status of the test chamber and facility. The target was a 5X-scale multi-shock shield supplied by NASA that was designed to fragment and catch the projectile. It consisted of seven bumper shields consisting of fiberglass (E-glass, #1, 2, 4, 5), stainless steel mesh (#3) and Kevlar (#6, 7) (Fig. 1) [19]. The target was 2.63 meters long and weighed about 700 lbs. The fiberglass bumpers were constructed from 22 layers of 26 oz./ft^2 FG-3784 satin weave E-glass fabric per bumper. The 304 stainless steel bumper was constructed from seven sheets of 304 stainless steel (SS) mesh. In contrast to the DebriSat and DebrisLV impact tests, no "soft catch " panels were installed. The materials used to fabricate the target are not representative of those on satellites or launch vehicle upper stages and the fact that it was designed to "catch" the projectile implies it may not be representative of a true hypervelocity impact.

A witness plate assembly was provided by Aerospace in order to collect debris for laboratory analysis, to identify materials produced by the impact and measure the albedo of debris (Fig. 2L). The witness plate assembly was located on the side of the chamber between the 3rd and 4th bumper shields (Fig. 3L). In the test the first four bumper shields were perforated by the projectile, the fifth was partially perforated and the frame was dislocated from the frame (Fig. 3R). The sixth shield (Kevlar) was deformed but was still intact [19]. We were not able to examine the remains of the target and debris in the chamber after the test. The witness plate assembly was shipped to Aerospace for analysis.

Exposed surfaces of the witness plate assembly were covered with a matte gray coating and fine debris (Fig. 2R). Larger deposits tended to be concentrated toward the down range side of the plate. The witness coupons located under the Whipple plates were relatively clean and uncoated compared to those which were uncovered (Fig. 4). This implies a highly directional nature to the impact deposits. Some of the material consists of loose micron- to nano-sized solidified molten droplets of an (Fe-Cr-Ni)-rich phase and an oxide/silicate phase (Fig 5L). The surface can be seen to be covered with small (< 1 μm) solidified molten droplets of the (Fe-Cr-Ni)-rich phase and larger droplets (to 100 μm) of the oxide/silicate (Fig. 5R). A loose flake of this material was potted in epoxy and sectioned and polished (Fig. 6). The material collected on the witness plate formed a thin continuous layer about 10-20 μm thick, solidified from molten droplets of the two phases that have a complex intermixed flow structure. The material consists of a crystalline (Fe-Cr-Ni)-rich phase and amorphous oxide/silicate phases [20].

The relative Fe-Cr-Ni proportions in the (Fe-Cr-Ni)-rich phase are not significantly different from the stainless steel bumper though it also contains significant amounts of Al and Si [20] (Fig. 7). The Al and Si contents are about equal in early arriving Fe-Cr-Ni while the later arriving Fe-Cr-Ni is Si rich and Al is low to absent. In the later droplets there is less flow structure and individual droplets tend to retain their shape implying they were already semi-solidified when deposited. The oxide phases have a range of compositions. The early oxide phase, mixed with (Fe-Cr-Ni)-rich phase in complex flow patterns, is primarily Al-Ca oxide with no Si (Fig. 7). The flow structures were produced by material which landed in a liquid form and then solidified. Later oxide droplets present on the surface are larger (to 200 μm) and show less flow structure but some gas bubbles. Later oxide droplets have significant Si and many have compositions similar to E-glass. The integrated (Ca-Al-Si) composition of the early phases with the complex flow patterns is significantly enriched in Al with respect to E-glass implying much of the Al (to 18%) came from the aluminum projectile. Aluminum has the lowest melting point of the starting materials. The first three bumpers that were perforated were fiberglass (1, 2) and stainless steel (3). Molten droplets consisting of Fe- Cr –Ni and Al-Ca oxide may have condensed from a mixed vapor phase formed from the bumpers and the projectile. Si and Al from the E-glass dissolved in the Fe-Cr-Ni leaving Al and Ca in an oxide phase. Additional Al came from the Al projectile. All Si may have dissolved in the (Fe-Cr-Ni)-rich phase possibly leaving no Si for the Al-Ca oxide. These droplets arrived first in a very fluid state and physically mixed and flowed together in complex patterns. The fourth and last bumper to be perforated by the decelerated projectile was E-glass. Molten droplets from this bumper arrived latter and some

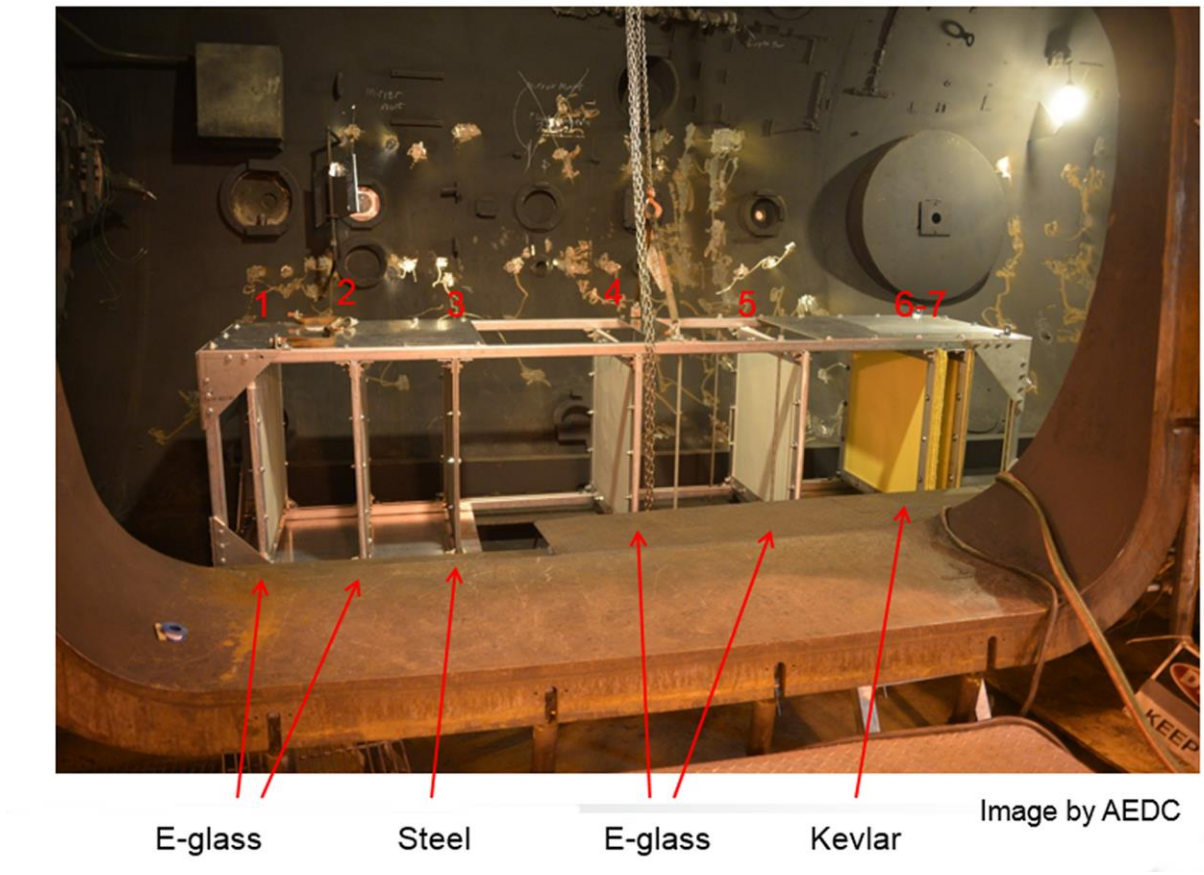

Fig. 1. Pre Preshot target with seven bumper shields being loaded into the AEDC test chamber. Projectile entry was from left to right.

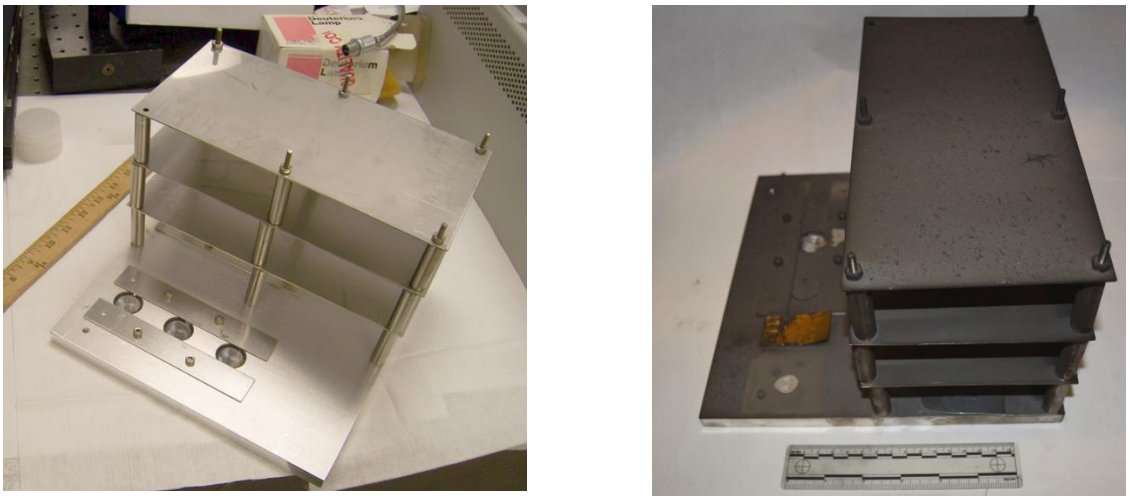

Fig. 2. Pretest witness plate assembly consisting of two sets of three 1" diameter fused quartz windows held down with stainless steel strips. One set of samples was fully exposed and the second set was protected under three steel Whipple plates (Left). Witness plate assembly post-test (Right).

Fig. 3. Pre Preshot target hanging in AEDC vacuum chamber looking down range. Witness plate assembly was mounted on the side of the chamber facing the target (Left). Target post-test looking down range. The fifth bumper shield is lying on the floor of the chamber (Right). Images by AEDC.

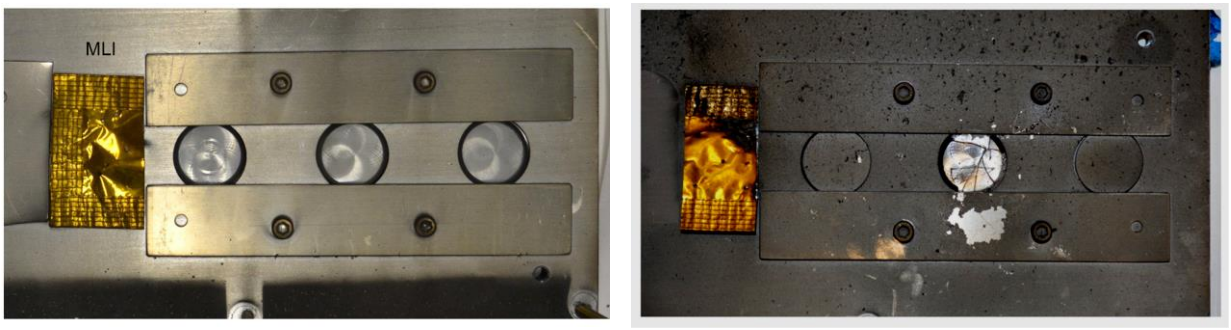

Fig. 4. Post-test witness samples. Coupons protected under Whipple plates; three 1" fused silica windows and Kapton multilayer insulation (MLI) (Left). Exposed coupons; center window has been broken and coating has flaked off lower hold-down strip and MLI (Right).

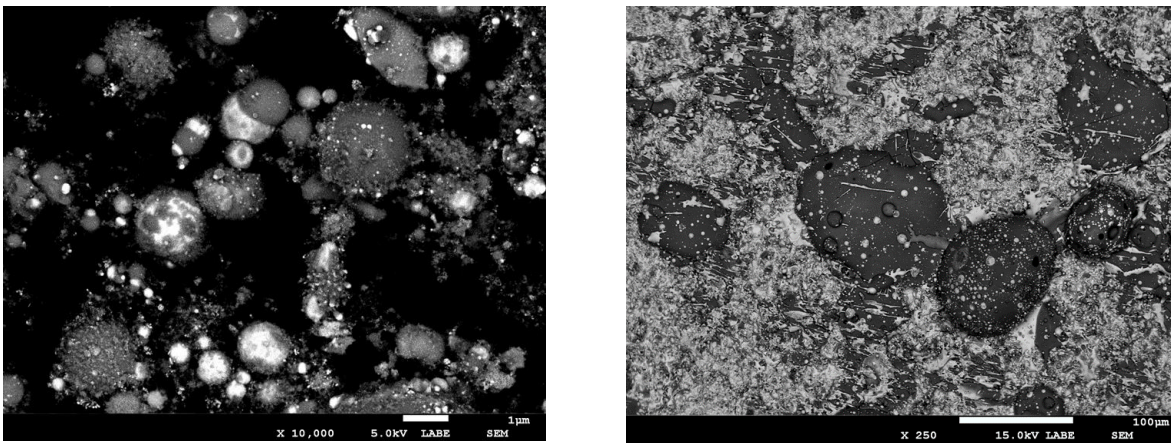

Fig. 5. Backscatter SEM image of loose solidified molten droplets removed from the surface of the witness plate by a tape lift (Left). Backscatter SEM image of surface of witness plate showing large solidified molten droplets of oxide/silicate and small droplets of a (Fe-Cr-Ni)-rich phase (Right).

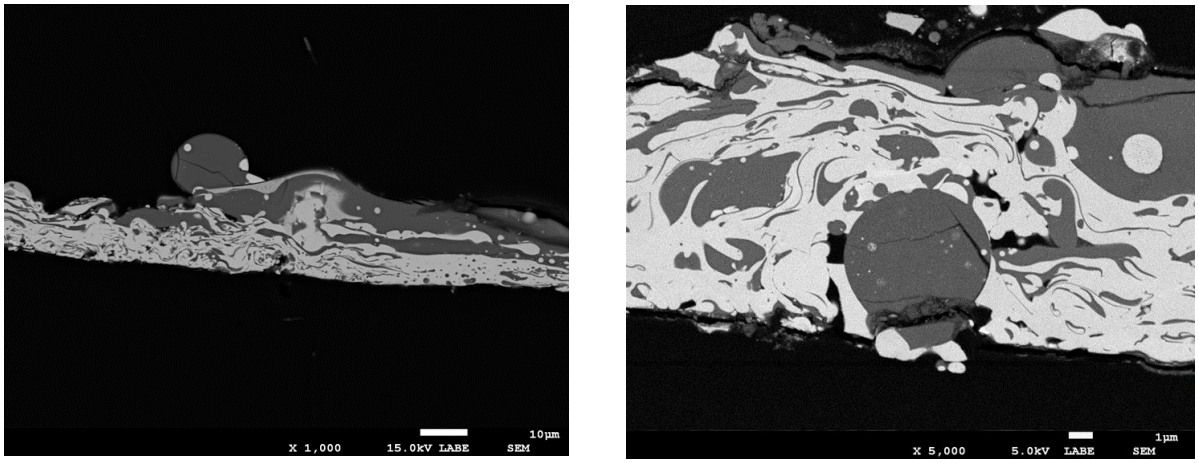

Fig. 6. Backscatter SEM images of polished cross section of solidified debris flake from the witness plate. Bottom of cross section was in contact with witness plate. The cross section preserves the time sequence of deposition. The bright areas are a (Fe-Cr-Ni)-rich phase – the dark areas are a Al-Ca oxide/silicate.

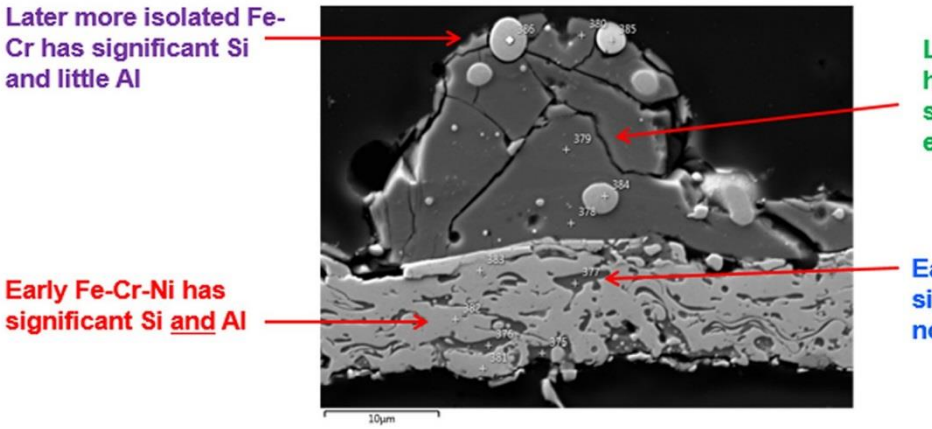

	375	376	377	378	379	380	381	382	383	384	385	386	E-Glass
O	56.19	59.88	60.02	61.11	61.70	60.28	3.51	2.83	2.75	2.22	3.83	4.39	65.3
Na				0.33									0.4
Mg				0.51	1.13	1.07							0.4
Al	27.13	27.81	28.24	16.62	12.94	19.01	12.29	14.63	2.19	1.20			5.9
Si	1.02			12.77	13.74	10.86	11.53	9.96	27.19	25.71	25.98	28.92	19.4
Ca	10.48	12.31	11.74	8.67	10.48	8.78							8.4
Cr	1.16						11.64	12.28	11.97	14.47	13.73	13.01	
Fe	4.01						53.60	49.74	46.72	47.92	48.52	47.63	
Ni	0.00						7.44	10.57	9.18	8.48	7.93	6.06	
Tot.	100.	100.	100.	100.	100.	100.	1000	100.	100.	100.	100.	100.	99.8

All values are atomic %

Fig. 7. EDS analyses of solidified molten deposits. Numbers in top row of table refer to analysis areas in image. E-glass composition is given for reference. Additional analyses presented in [20].

were less fluid and show less flow structure. The droplet size was larger (to 200 µm) and the composition was more consistent with E-glass. The later droplets show little to no mixing and the late Fe-Cr-Ni droplets retain their shape. This implies they were cooler and partially solidified when deposited.

There was a drop in FTIR reflectance from 90-95% for unexposed surfaces to 20-25%, for exposed surfaces as a result of impact (Fig. 8L). The deposition on the witness plate assembly appears to be line of sight since the underside of the Whipple shield showed much less of a change (67-85%). FTIR spectral features from the

deposited material are related to silicate (1080 cm^{-1}) and borate (1400 cm^{-1}) from the E-glass bumpers that were penetrated (Fig. 8R). The silicate feature shifted as a result of a change in composition.

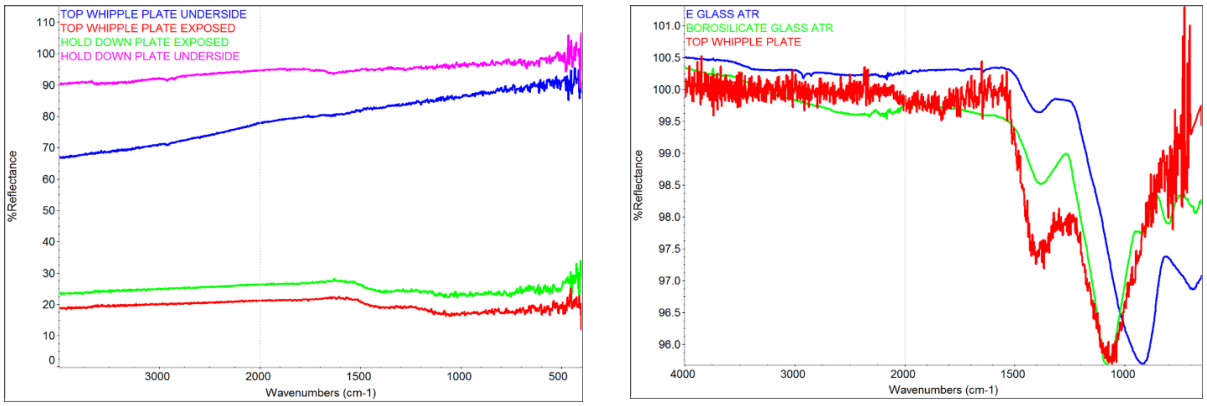

Fig. 8. Hemispherical FTIR reflectance spectra of witness plate surfaces (left). Attenuated total reflectance FTIR spectra of witness plate surface compare with E-glass and borosilicate glass (right).

3. DEBRISLV TEST

The 15 kg DebrisLV target was constructed from materials representative of a launch vehicle (LV) upper stage [21]. It consisted of two tanks, the larger being constructed from 5154-aluminum and filled with 15 psi Xe, and the smaller from titanium, which was part of a nutation control thruster assembly, and contained 65 psi He [22]. Additional materials included: an external 6061-aluminum skin, 304 stainless steel and copper longerons, stainless steel tubing and two small strap-on aluminum tanks (Fig. 9). The impact chamber was lined with soft catch foam in order to trap impact fragments for size distribution and trajectory analysis [5, 7, 9] (Fig. 9L). Additional witness plates were placed in the chamber in order to capture impact debris for analysis to determine the cause of debris darkening. The witness plate assembly (Fig. 10L) was similar to that in Pre Preshot, but included aluminum and NaCl disks in addition to fused silica, and was placed 3 meters up range from the target in order to not interfere with the soft catch foam system (Fig. 10R). Twenty-four SEM stub witness plates were also placed on the surface of the soft catch panels [23] (Fig. 9L).

The test was conducted April 1, 2014. Large fragments were returned to Aerospace for examination while the soft catch panels have been stored by the University of Florida. After impact the majority of the DebrisLV main tank remained in one piece and the interior was coated with a thin layer (50-100 µm) of solidified molten material consisting primarily of crystalline aluminum (Fig. 11). The layer was loosely adhered and tended to flake off in large pieces which are an unexpected source of untrackable orbital debris [22, 23]. The surface of the tank was coated with a thin dark deposit consisting of disordered graphitic carbon and solidified nano droplets of Al, Fe and Cu. SEM witness stubs, witness plate asembly and DebrisLV fragments were black in color and were contaminated with < 1mm soft catch foam fragments (Fig. 12). The majority of the SEM stubs were dislodged from the soft catch during the impact. Those that remained intact were uprange of the target. The SEM stubs also had a thin film of condensed soft catch vapor based on FTIR analyses of stubs that had loose soft catch fragments removed by rinsing with isopropyl alcohol (Fig. 13). The FTIR spectra of the stubs were very similar to condensate of soft catch heated to 1000 ºC in a tube furnace. In high speed camera video it can be seen that the high temperature plasma flash produced by the impact completely fills the chamber contacting the soft catch [21]. In contrast, the black deposits on the large tank fragment showed little soft catch condensate. Deposits on SEM stubs and witness plates are predominantly carbon (Table 2) and consist of agglomerates of micro to nano-sized carbonaceous material with a moss-like appearance that was derived from the soft catch (Figs. 14, 15). Disordered graphitic carbon is also present based on Raman spectra (Fig. 13R) and distorted transmission electron microscope (TEM) lattice fringe images (Fig. 16R). Nano droplets of

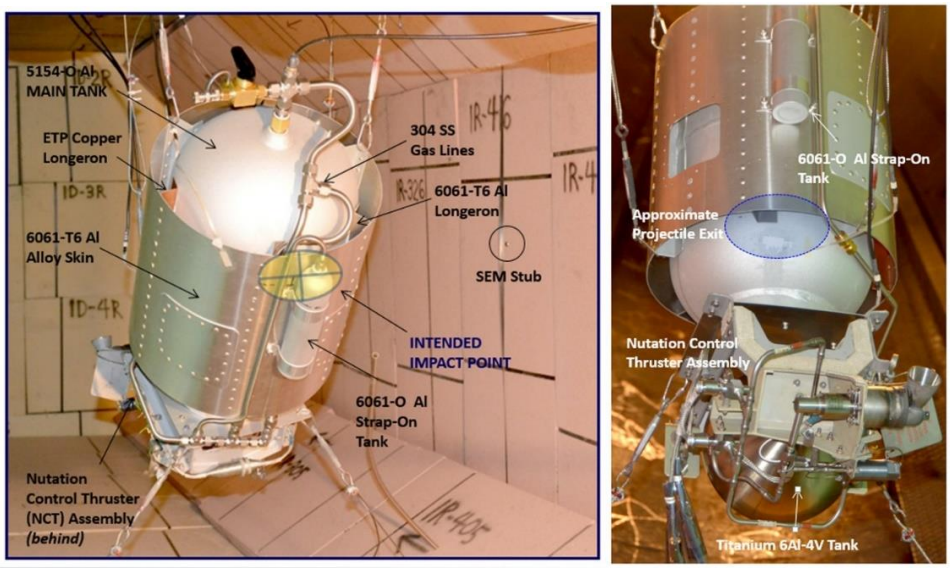

Fig. 9. DebrisLV target in vacuum chamber lined with soft catch foam. View looking down range. SEM stubs (circle) were placed in the soft catch foam (Left). View of target looking uprange showing nutation control thruster assembly (Right).

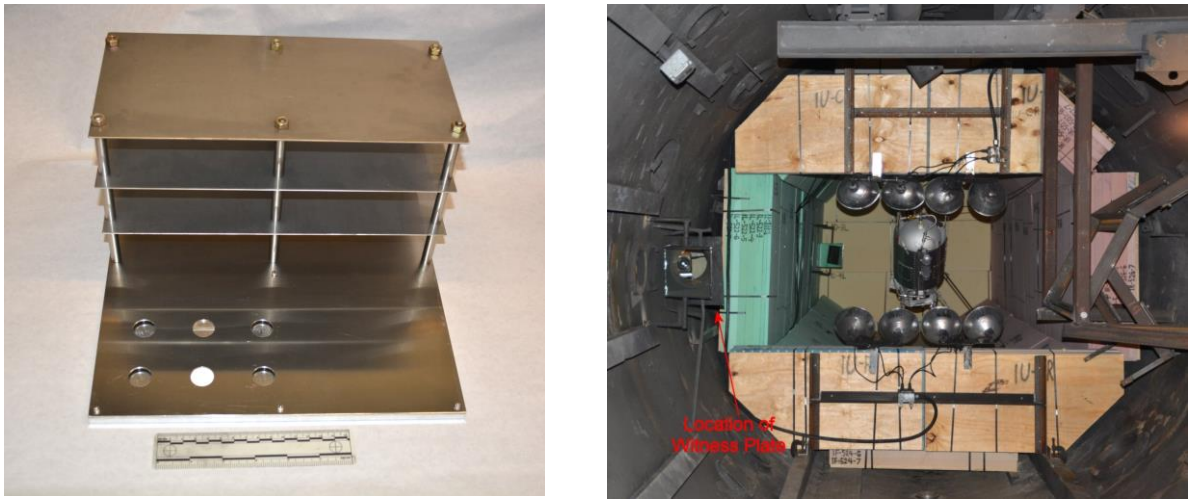

Fig. 10. Witness plate assembly – pretest (Left). Location of witness plate assembly with respect to DebrisLV target. Flash lamps and debris dams are uprange of the target (top and bottom) (Right).

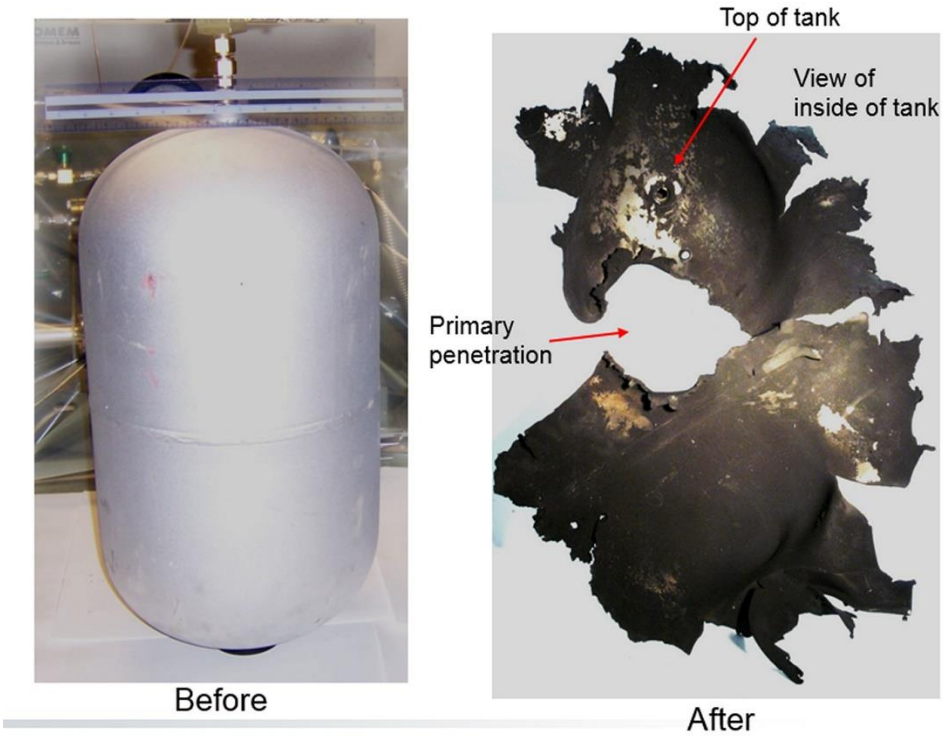

Fig. 11. Comparison of 30 cm diameter internal aluminum tank before and after hypervelocity impact. Interior and exterior of tank fragments were covered with a thin black soot-like deposit.

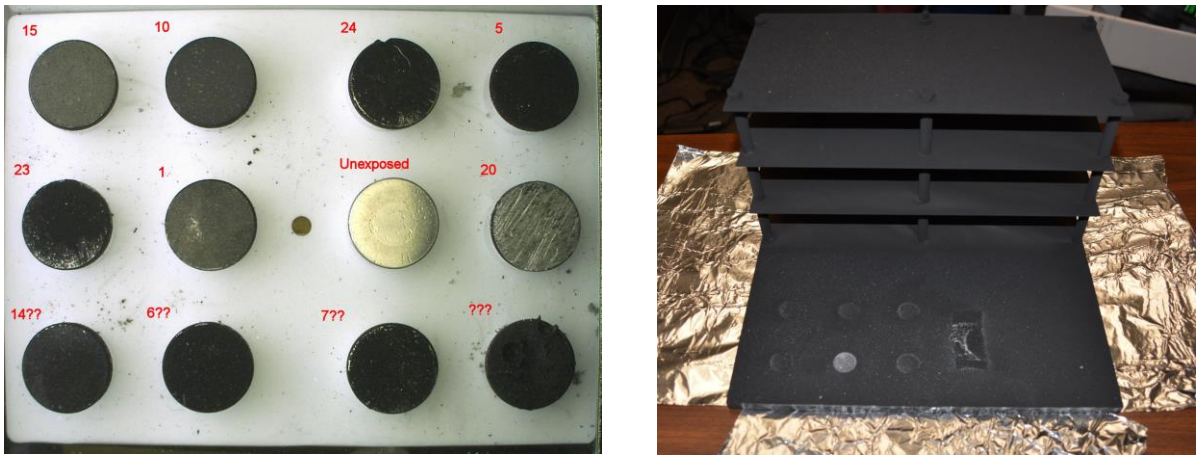

Fig. 12. SEM stub witness plates (1 cm diameter) with black coatings after impact (Left).
Witness plate assembly post-test, compare with Fig. 9 (Right).

metallic materials (Al, Fe, Cu) and filamentous structures were present indicating melting of target components as a result of the impact (Fig. 14-16). The mean particle size was on the order of 0.20 μm. The aluminum is often present in the form of an oxide based on EDS analyses. Many of the < 200 nm metallic particles are single crystals based on TEM lattice fringe images (Fig. 16R).

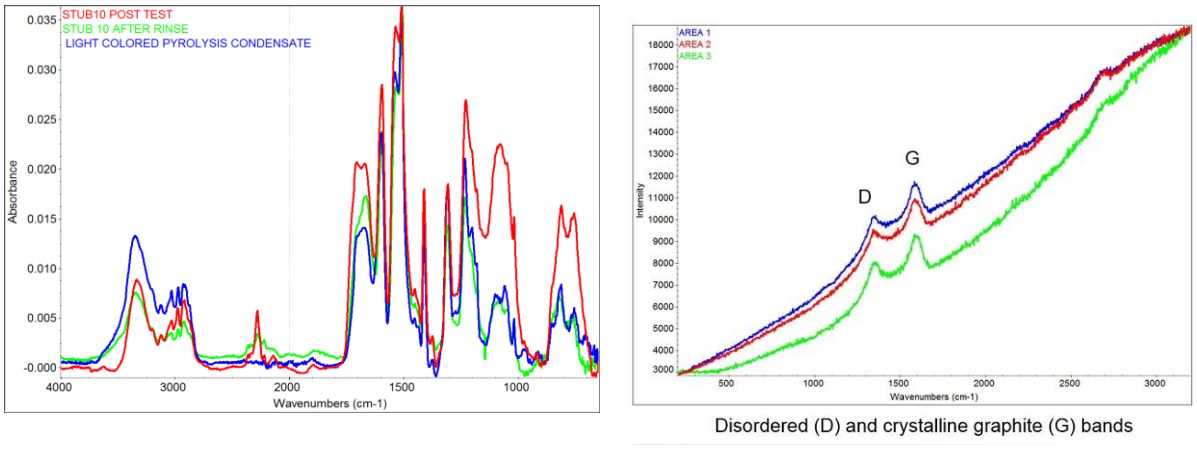

Fig. 13. FTIR diffuse reflectance spectra comparing experimentally produced soft catch foam pyrolysis condensate and deposits on SEM stubs (before and after rinsing with isopropyl alcohol) (Left). Raman spectra of deposits on witness plate assembly support post showing disordered (D) and graphitic (G) carbon peaks (Right).

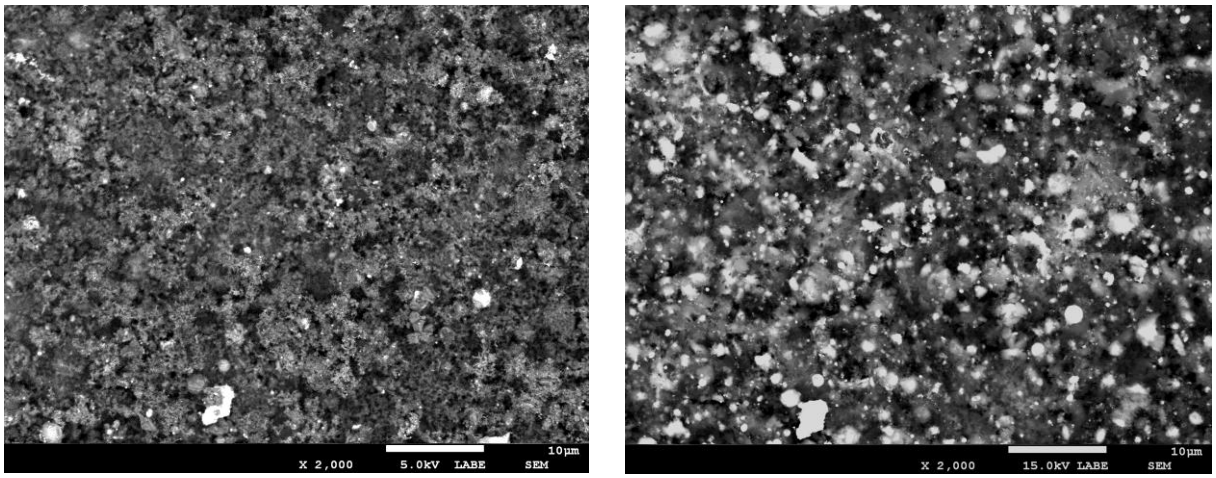

Fig. 14. Backscatter SEM images of micro to nano-scale impact deposits on SEM stub witness plate (5 KV) (Left). Same view as on left but with 15KV – note that additional high-Z particulates containing Al, Fe, Cu (bright) are visible with greater penetration depth (Right).

Table 2. Average elemental composition (atomic %) of deposits from 8 SEM stubs.

C	O	Mg	Al	Si	P	Ca	Cr	Fe	Cu	Zn	Total
67.8	14.1	1.2	15.3	0.1	0.3	0.1	0.1	0.9	0.1	0.1	100.1

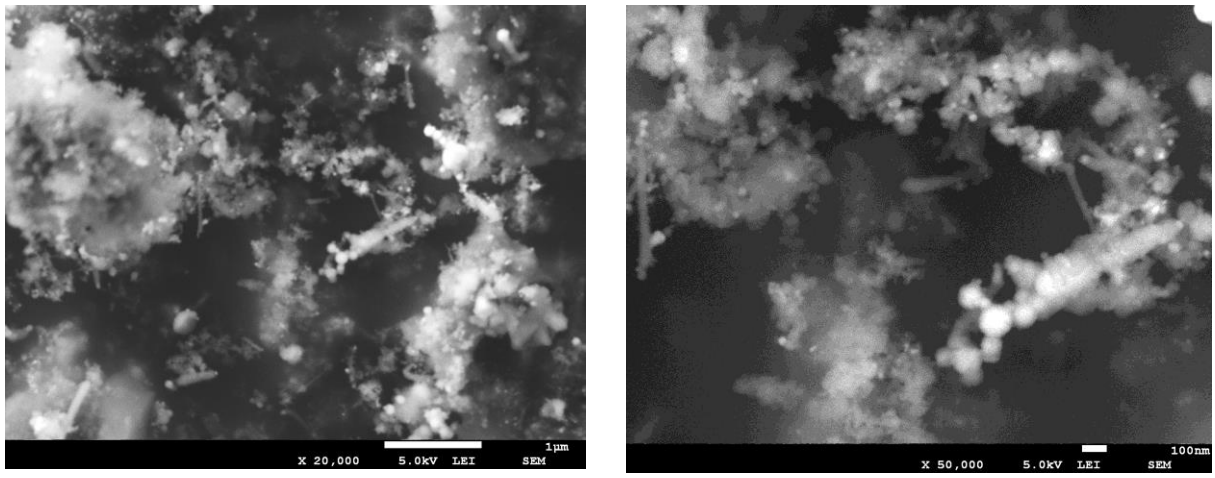

Fig. 15. Secondary SEM images of nano-scale impact deposits on SEM stub witness plate. Note solidified spherical droplets and filamentous structures.

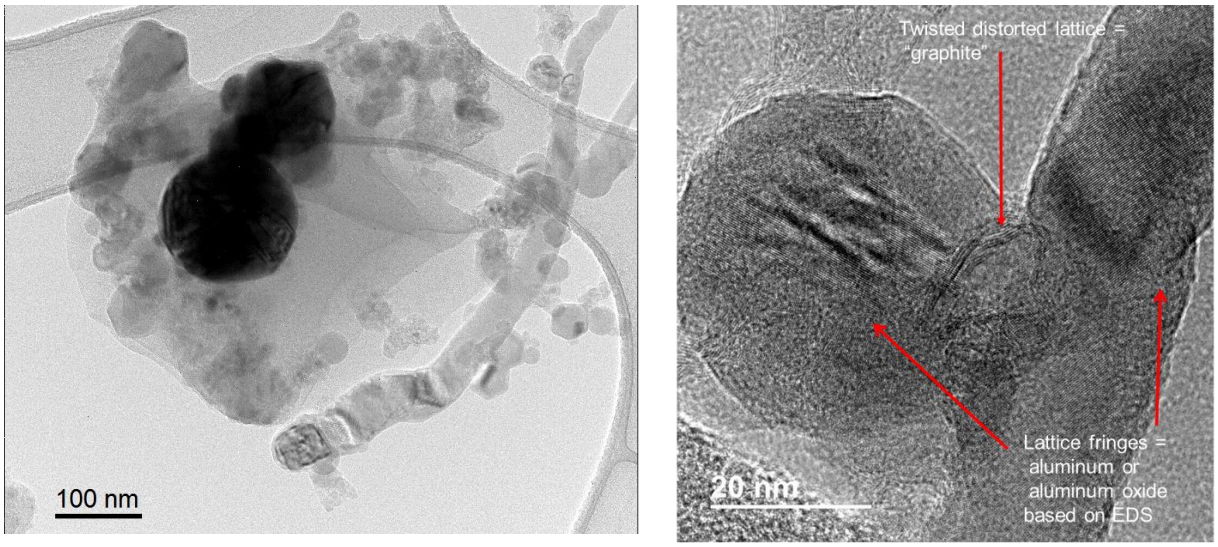

Fig. 16. TEM images of nano-sized filaments and particulates from SEM stub witness plate on lacey carbon support (Left). High resolution TEM image of particulate and filament showing lattice fringes (Right).

Witness plates and tank fragments show a significant decrease in reflectance (from 95% to 6%) (Fig. 17L). Soft catch contamination was seen in FTIR reflectance spectra of SEM stubs and witness plates. As a result, it was not possible to get a clean spectrum of the debris generated by the hypervelocity impact. An additional band at 800 cm^{-1}, probably from an aluminum oxide, was seen on some of the samples [18] (Fig. 17R). The location of this feature does not correspond to normal stoichiometric aluminum oxide but does resemble non-stoichiometric Al-oxide nano-clusters produced by sputtering [24]. The only source of the oxygen in the test was residual air in the chamber (~2 Torr) and would not be expected on orbit. This has been confirmed by recent laboratory laser ablation simulations of hypervelocity impacts with aluminum which produced debris coatings very similar to those observed in the DebrisLV and DebriSat tests [25, 26].

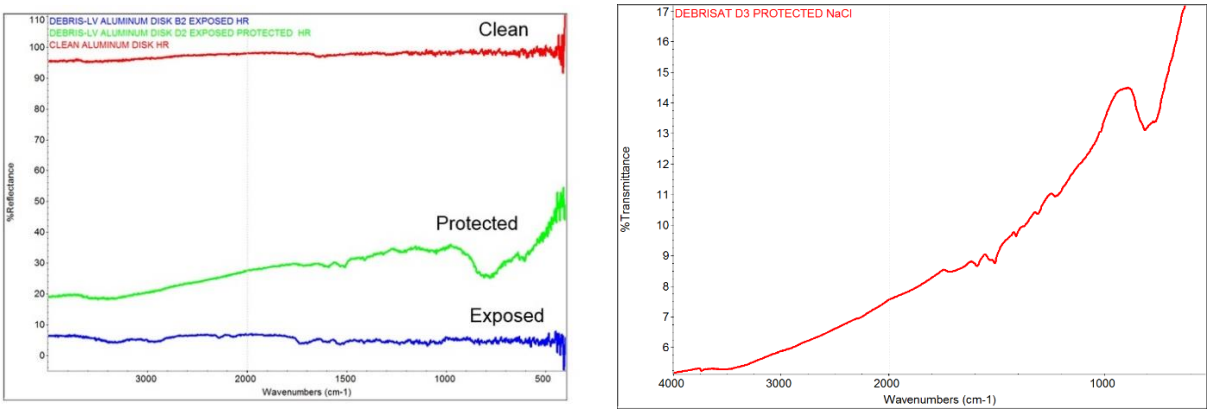

Fig. 16. FTIR hemispherical reflectance spectra of impact deposits on witness plate assembly aluminum disk (Left). FTIR transmission spectrum of impact deposit on witness plate assembly NaCl window showing soft catch (1600-1200 cm^{-1}) and suspected aluminum oxide (800 cm^{-1}) peaks (Right).

4. DEBRISAT TEST

The DebriSat test was conducted to better understand the distribution of fragments generated from a hypervelocity impact with a modern satellite [1]. The 50 kg target was a constructed by the University of Florida from materials representative of a modern LEO satellite (Fig.18) [7, 21]. The Aerospace Corporation Concept Design Center advised on the selection of materials for various subsystems. This included components representative of solar panels, composite overwrap pressure vessel (COPV), carbon fiber composites, aluminum honeycomb panels, multilayer insulation (MLI), solenoids, printed circuit boards and optics. As in the DebrisLV test the chamber was lined with soft catch panels and the same witness plate assembly and SEM stubs were used [27]. The test was conducted April 15, 2014. The recovery and study of impact generated fragments down to 2 mm is an ongoing effort at the University of Florida [28-30].

The results from our examination of the witness plates were similar to those from the DebrisLV test [27]. The SEM stubs, witness plate assembly and DebriSat fragments were covered with black soot and were contaminated with soft catch foam fragments. The SEM stubs and witness plate assembly discs were also covered with a thin film of condensed soft catch vapor, similar to that seen with the DebrisLV test. Deposits on the SEM stubs and witness plate assembly were on the order of 2-4 μm thick and are predominantly carbon and consist of agglomerates of nano carbonaceous material. (Table 3). Fluorine from Teflon wire insulation was also common in the SEM stub and witness plates deposits. Nano droplets of metallic materials (Al, Fe, Cu, Zn, Ge) were also present indicating melting as a result of the impact (Fig. 19, 20L). Aluminum was from the Al honeycomb, nadir and zenith panels, structural core and COPV liner. Aluminum oxide particles were also present. Iron was from stainless steel tubing and solenoids. Germanium was from the solar cells and copper was from wiring and solenoids. The source of the zinc has not been identified. The solidified molten nano metal droplets are crystalline based on TEM lattice fringes and consist of only a few crystallites. Carbonaceous deposits are primarily from the soft catch (similar to DebrisLV) though the C-C composite honeycomb face sheets and MLI are also possible sources. Disordered graphitic carbon is present based on Raman spectra and TEM wrinkled lattice fringes (Fig. 20R). The witness plate assembly was covered in a black layer of loose “soot”, even under the protective Whipple plates.

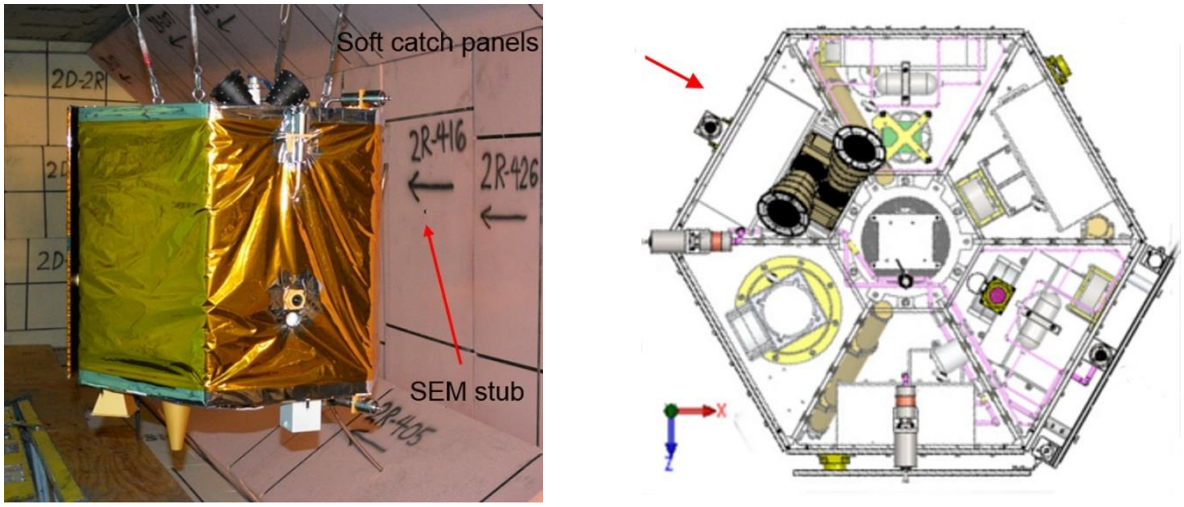

Fig. 18. DebriSat target hanging in the vacuum chamber looking down-range prior to the test (Left). Schematic transverse cross section of DebriSat showing diverse compartmentalized structure of target and direction of projectile entry (red arrow) [1] (Right).

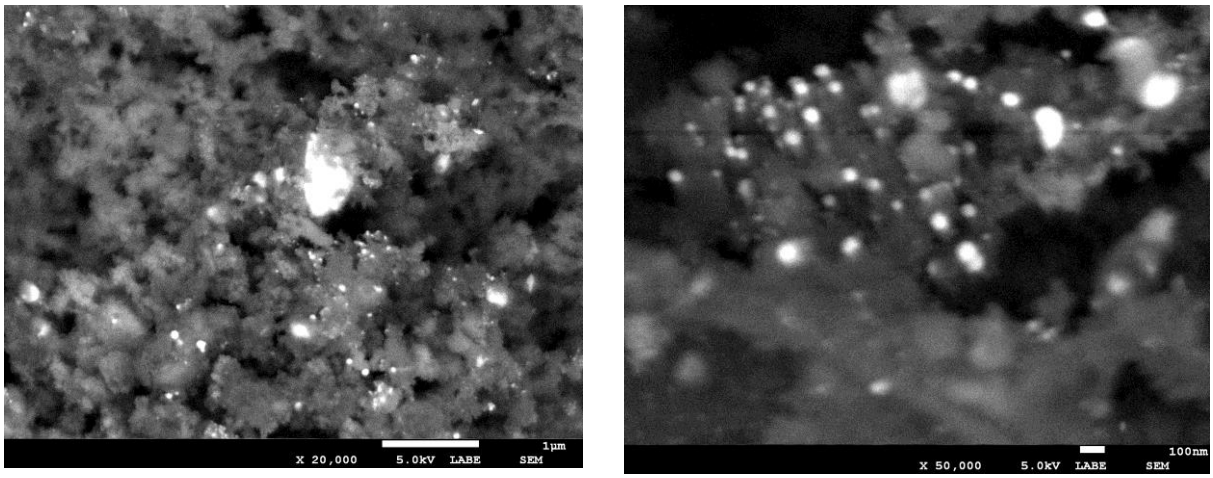

Fig. 19. Backscatter SEM images of deposits on SEM stubs. Bright objects are higher-Z (Al, Fe, Cu).

Table 3. Average EDS analyses (atomic %) of deposits from five SEM stubs.

C	O	F	Na	Mg	Al	Si	P	Cl	Cr	Fe	Cu	Zn	Ge	Total
64.1	16.6	4.4	0.3	0.3	7.2	0.6	0.2	0.1	0.1	0.6	0.4	3.0	0.1	98.0

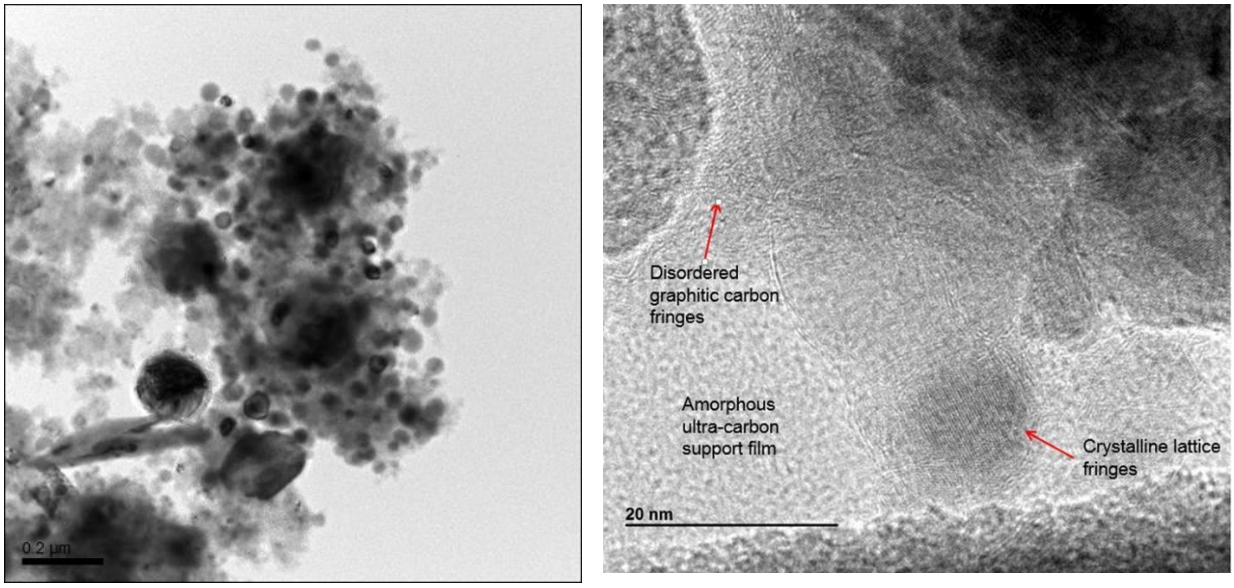

Fig. 20. TEM images of nano-deposits consisting of crystalline Al, Al-Oxide and disordered graphitic carbon.

The witness plates show a significant decrease in FTIR hemispherical reflectance from 95% to 6% (Fig. 21). Soft catch contamination was seen in the FTIR reflectance spectra of DebriSat fragments, SEM stubs and witness plate. As a result, it was not possible to get a clean spectrum of the debris generated by the hypervelocity impact. An additional "oxide" band, which may be from a form of aluminum oxide, was seen on some samples (Fig. 21R).

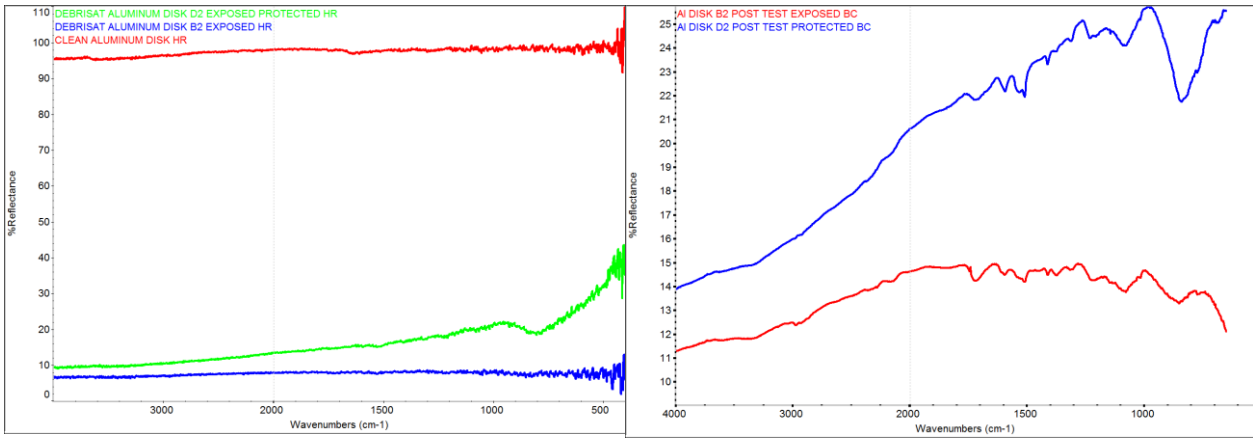

Fig. 21. FTIR hemispherical reflectance spectra of witness plate deposits (Left). Qualitative biconical FTIR reflectance spectra of witness plate showing soft catch (1800-1000 cm^{-1}) and possible aluminum oxide (800 cm^{-1}) absorption bands (Right).

5. SUMMARY AND CONCLUSIONS

The main objectives of this study were to collect microscopic debris coatings from hypervelocity impacts for analysis in the laboratory to determine their physical characteristics (particle size distribution, chemistry and optical properties) and make direct albedo measurements. While soft catch contamination from the DebrisLV and DebriSat tests prevented clean observations of the hypervelocity impact debris it was still possible to obtain valuable information related to the observed impact deposits under low-vacuum conditions.

In all three tests the witness plates, and in many cases target fragments, were coated with thin coatings (2-20 μm) of impact debris. While not representing a large volume they had a significant influence on the reflectance/albedo of the surfaces they covered. The debris from the Pre Preshot test consisted of a two-phase mixture formed from solidified molten silicate and steel droplets. Individual droplets ranged from 100 μm to 10 nm. The reflectance of witness plates dropped from 95% to 20-30% as a result of the debris. Debris collected on witness plates in the DebrisLV and DebriSat tests consisted of μm to nm-sized solidified molten metallic and oxide droplets in a matrix of condensed vaporized soft catch. Disordered graphitic carbon was also detected. The reflectance of debris-covered witness plates dropped from 95% to 5%. The dramatic decrease in reflectance for hypervelocity impact debris is attributed to the effect of scattering from μm to nm-sized solidified molten metallic droplets and the presence of graphitic carbon, when organics are present. The presence of soft catch in the later tests and the high organic content with graphitic carbon in the debris appear to be responsible for this much lower post-test reflectance. While soft catch foam is not present in satellites, other organic materials such as MLI blankets, carbon-fiber reinforced composites, printed circuit boards and wire insulation may similarly produce disordered graphitic carbon in hypervelocity impacts resulting in very low albedos. These results confirm those in [11] (Table 1) where very low albedos (~ 0.05) were measured from orbital debris, though they qualified their results as possibly being low by a factor of 2X. The presence of micro to nano-sized particulates produced by these hypervelocity impacts tests confirms them as a source for micro debris wakes [31].

A suspected aluminum oxide band was observed on some witness plates from the DebrisLV and DebriSat tests and was corroborated by EDS analyses of some particulates. This may have resulted from residual oxygen (air) in the vacuum chamber and would not be expected on-orbit. The presence of residual air in the chamber and Xe in the main DebrisLV tank may have also contributed to the formation of nano-particulates through collisional cooling of the vapor phase produced by the impact. Recent laboratory laser ablation simulations of hypervelocity impacts with aluminum have produced debris coatings very similar to those observed in the DebrisLV and DebriSat tests [25, 36] and have demonstrated that aluminum oxide forms under vacuum conditions (~2 Torr air) comparable to DebrisLV/DebriSat and that it does not form under high vacuum equivalent to LEO.

6. ACKNOWLEDGEMENTS

We thank the DebriSat team members for their support during the tests: J.-C. Liou (NASA Space Debris Program Office, NASA JSC), Norman Fitz-Coy (U. of Florida); Heather Cowardin and John Opiela (ESCG/Jacobs); the AEDC Range G Light Gas Gun Staff and Charles Griffice and Marlon Sorge (Aerospace). Financial support was provided by: Charles Griffice (Aerospace) and Thomas Huynh (SMC/EN). V. Sather is thanked for reviewing an early version of this paper.

7. REFERENCES

1. Liou, J.-C., Clark, S., Fitz-Coy, N., Huynh, T., Opiela, J., Polk, M., Roebuck, B., Rushing, R., Sorge, M. and Werremeyer, M., DebriSat – A planned laboratory-based satellite impact experiment for breakup fragment characterization, Proc. 6th Europe. Conf. Space Debris, Darmstadt, Germany, 2013.
2. Hogg, D.M, Cunningham, T.M, Isbell, W.M, Final report on the SOCIT series of hypervelocity impact tests. Wright Laboratory WL-TR-93-7025, General Research Corporation, Santa Barbara, CA, USA, 1993.
3. McKnight, D. S., Johnson, N. L., Fudge, M. L. and Maclay, T. D., Satellite orbital debris characterization impact test (SOCIT) series data collection report, Kaman Sciences Corporation, Contract No. NA 9-19215, 1995.
4. Krisko, P. H., Horstman, M. and Fudge, M. L., SOCIT4 collisional-breakup test data analysis: With shape and materials characterization, Advances in Space Research 41, 1138–1146, 2008.
5. Ausay. E., Cornejo, A., Horn, A., Palma, K., Sato, T., Blake, B., Pistella, F., Boyle, C., Todd, N., Zimmerman, J., Fitz-Coy, N., Liou, J.-C., Sorge, M., Huynh, T., Opiela, J., Krisko, P. and Cowardin, H., A comparison of the SOCIT and DebriSat experiments, 7th Europe. Conf. Space Debris, Darmstadt, Germany, 2017.
6. Johnson, N. L., Krisko, P., Liou, J.-C. and Anz-Meador, P. D., NASA's new breakup model of EVOLVE 4.0, Adv. Space Res., 28, 1377-1385, 2001.
7. Polk, M., Woods, D., Roebuck, B., Opiela, J., Sheaffer, P and Liou, J.-C., Orbital Debris Assessment Testing in the AEDC Range G, Procedia Engineering, 103, 490 – 498, 2015.
8. Polk, E. M. and Roebuck, B. E., DebriSat Hypervelocity Impact Test , Arnold Engineering Development Center AEDC-TR-15-S-2, 2015, www.dtic.mil/get-tr-doc/pdf?AD=ADA625195
9. DebriSat Soft-Catch Panel Impact Test, NASA Orbital Debris Quarterly News, Vol. 18(1), 4-5, 2014.
10. Mulrooney, M. K., Matney, M. J., Hejduk, M. D. and Barker, E. S., An Investigation of Global Albedo Values, Proceedings 2008 AMOS Technical Conference, Wailea, HI, 719-728, 2008.
11. Potter, A. E., Henize, K. G. and Talent, D. L., Albedo estimates for debris, in Orbital debris from upper-stage breakup (ed. J. P. Loftus, Jr.) Progress in Astronautics and Aeronautics, 121, 147-156, 1989.
12. Henize, K. G. and Stanley, J. F., Optical observations of space debris, AIAA/NASA/DOD Orbital Debris Conference: Technical Issues & Future Directions, Baltimore, MD, AIAA-90-134O, 1990.
13. Lebofsky, L. A. and Vilas, F., Thermal models applicable for visual and infrared studies of orbital debris, Adv. Space Res., 10, 377-380, 1990.
14. Henize, K. G., O'Neill, C. A., Mulrooney, M. K, and Anz-Meador, P., Optical properties of orbital debris, J. Spacecraft Rockets, 31, 671-677, 1994.
15. Kessler, D. J. and Jarvis, K. S., Obtaining the properly weighted average albedo of orbital debris from optical and radar data, Advances in Space Research, 34, 1006-1012, 2004.
16. Mulrooney M. and Matney, M., Derivation and Application of a Global Albedo Yielding an Optical Brightness to Physical Size Transformation Free of Systematic Errors, Proceedings 2007 AMOS Technical Conference, Kihei, HI, 719-728, 2007.
17. Mulrooney, M., Matney, M. and Barker, E. A New Bond Albedo for Performing Orbital Debris Brightness to Size Transformations., 2008 International Astronautical Congress, Glasgow, Scotland, 2008.
18. Adams, P. M., Sheaffer, P. M. and Radhakrishnan, G., FTIR Analyses of Hypervelocity Impact Deposits: DebriSat Tests, Aerospace Report No. TOR-2015-00941, 2015, http://www.dtic.mil/get-tr-doc/pdf?AD=ADA627320
19. Christiansen, E., A. Davis, A., Miller, J. and Lear, D., Hypervelocity Impact Test with Large Mass Projectile, NASA Orbital Debris Quarterly News, Vol. 18(2), 6-7, 2014.
20. Adams, P. M. and Sheaffer, P. M., DebriSat Pre Preshot Laboratory Analyses, Aerospace Report No. TOR-TOR-2014-03083, 2014, http://www.dtic.mil/get-tr-doc/pdf?AD=ADA627557
21. Liou, J.-C., Opiela, J., Cowardin, H., Huynh, T., Sorge, M., Griffice, C., Sheaffer, P., Fitz-Coy, N., Wilson, M., Rushing, R., Hoff, B., Nolen, M., Polk, M., Roebuck, B and Woods, D. Successful Hypervelocity Impacts of DebrisLV and DebriSat, NASA Orbital Debris Quarterly News, Vol. 18(3), 3-5, 2014.
22. Sheaffer, P. M. and Adams, P. M., DebrisLV Hypervelocity Impact Post-Shot Physical Results Summary, Aerospace Report No. TOR- 2014-03577, 2015, http://www.dtic.mil/get-tr-doc/pdf?AD=ADA625015
23. Adams, P. M., Sheaffer, P. M., Lingley, Z. and Radhakrishnan, G., Debris-LV Laboratory Analyses, Aerospace Report No. TOR-2015-00928, 2015.

24. Polonskyi, O., Kylián, O., Kousal, J., Solař, P., Artemenko, A., Choukourov, A., Slavínská, D. and Biederman, H., Aluminium oxide clusters and their nanocomposites with plasma polymers prepared by a gas aggregation cluster source and plasma polymerization, 19th International Symposium of Plasma Chemistry, Bochum, Germany, 2009.
25. Radhakrishnan, G., Adams, P. M., Panetta, C. J. and Alaan, D. R., Laboratory Comparisons to Hypervelocity Impact and Debris Darkening, Procedia Engineering, (in press), 2017.
26. Radhakrishnan, G., Adams, P. M., Alaan, D. R and Panetta, C. J., Debris Albedo from Laser Ablation in Low and High Vacuum: Comparisons to Hypervelocity Impact, 2017 AMOS Technical Conference Proceedings, Maui, HI, *in preparation for this conference.*,2017.
27. Adams, P. M., Lingley, Z., Presser, N. and Radhakrishnan, G, DebriSat Laboratory Analyses, Aerospace Report No. TOR-2015-00876, 2015, http://www.dtic.mil/get-tr-doc/pdf?AD=ADA625039
28. Rivero, M., Kleespies, J., Patankar , K., Fitz-Coy, N., Liou, J.-C., Sorge, M., Huynh, T., Opiela, J., Krisko, P. and Cowardin, H., Characterization of debris from the DebriSat hypervelocity test, Proceedings 66th International Astronautical Congress, Jerusalem, Israel, IAC-15-A6.29x30343, 2015.
29. Rivero, M., Shiotani, B., Carraasquilla, M., Fitz-Coy, N., Liou, J.-C., Sorge, M., Huynh, T., Opiela, J., Krisko, P. and Cowardin, H., DebriSat fragment characterization system and processing status, Proceedings 67th International Astronautical Congress, Guadalajara, Mexico, 2016.
30. Cowardin, H., Liou, J.-C., Anz-Meador, P., Sorge, M., Opiela, J., Fitz-Coy, N., Huynh, T. and Krisko, P., Characterization of orbital debris via hyper-velocity laboratory based tests, 7th Europe. Conf. Space Debris, Darmstadt, Germany, 2017.
31. Maclay, T. D. and McKnight, D., The contribution of debris wakes from resident space objects to the orbital debris environment, IAA.6.4-94-692.

,